Review Article ISSN 2689-1050

Chemical & Pharmaceutical Research

Structure, Quantum Chemical and In Silico Molecular Docking Analysis of some Di-Ortho-Substituted Halogenated Biphenyls

Neha Kumari[1], Ruchika Sharma[1], Mulveer Singh[1], Jayakumar Mohan Raj[2], Saminathan Murugavel[2], Sonachalam Sundramoorthy[3], and Rajni Kant[1*]

[1]*Chemical Crystallography Laboratory, Department of Physics, University of Jammu, Jammu Tawi–180006, Jammu & Kashmir (UT), India.*

[2]*Department of Physics, Thanthai Periyar Government Institute of Technology, Vellore- 632002, Tamil Nadu, India.*

[3]*Department of Physics, Agni College of Technology, Old Mahabalipuram Road, Thalambur, Chennai-600130, Tamil Nadu, India.*

[*]Correspondence:
Rajni Kant, Chemical Crystallography Laboratory, Department of Physics, University of Jammu, Jammu Tawi-180006, India, Tel/Fax [O]: +91 191 243 2051.

Received: 24 Jul 2022; **Accepted:** 10 Sep 2022; **Published:** 16 Sep 2022

Citation: Kumari N, Sharma R, Singh M, et al. Structure, Quantum Chemical and In Silico Molecular Docking Analysis of some Di-Ortho-Substituted Halogenated Biphenyls. Chem Pharm Res. 2022; 4(3): 1-9.

ABSTRACT

The structures of three di-ortho-substituted halogenated biphenyls have been revisited for their optimized geometry and other quantum chemical investigations. The X-ray data, in conjunction with quantum chemical investigations, reveals some interesting results. The Hirshfeld surface analysis helps visualize various intermolecular interactions and the energy frameworks dwell further on the dominant interaction energy component for each structure. To study the inhibitory behaviour of each biphenyl against Cytochrome-P450-14alpha-sterol demethylase fungal enzyme (PDB code: 1EA1), the results of molecular docking studies suggest that the di-ortho-substituted halogenated biphenyls may be regarded as effective and efficient antifungal drugs.

Keywords

Density functional theory, Hirshfeld surface analysis, Interaction energy, Mulliken charges, Molecular docking.

Introduction

Biphenyls are an important intermediate in organic chemistry that serves as the structural moiety in a wide range of compounds with significant biological activities [1]. Being a neutral molecule, it is least reactive and required to be functionalized by the introduction of some active groups [2]. Substituted biphenyls have been reported as important pharmacologically important molecules exhibiting sufficient antifungal activity [3]. These molecules have caught the interest of researchers, particularly for their molecular geometry, crystallization behaviour, crystal packing, thermal motion analysis, the torsion around the biaryl bond (that is considered to have a significant impact on bioactivities of biphenyls) [4,5] and their coplanar conformation in the crystalline state at room temperature (indicating a dihedral twist of ~ 44º in the gas phase) [6].

Halogenated-substituted biphenyls have been extensively used as an industrial intermediate in the production of heat transfer fluids, in the synthesis of chemical compounds, formulations for dye carriers in textile dyeing and pesticides in the form of PCB (Polychlorinated biphenyl). These are reportedly being used in medical chemistry for antimicrobial, antifungal, antidiabetic, analgesic, anti-inflammatory activities, etc [7-10]. In view of some wide-ranging applications of ortho-substituted halogenated biphenyls, the theoretical studies (DFT, Hirshfeld surface, energy frameworks, and molecular docking) on three CSD- mined crystal structures of biphenyls, (M-1) 2,2'difluorobiphenyl (CSD code: PUGPIQ), (M-2) 2,2'dichlorobiphenyl (DCLBIP) and (M-3) 2,2'bromobiphenyl (HIQQON), have been reported. The X-ray crystallographic structures of these three chemically-similar-looking structures [11-13] have been identified from the CSD database (*version:* 2022) and their chemical structures are presented in Figure 1.

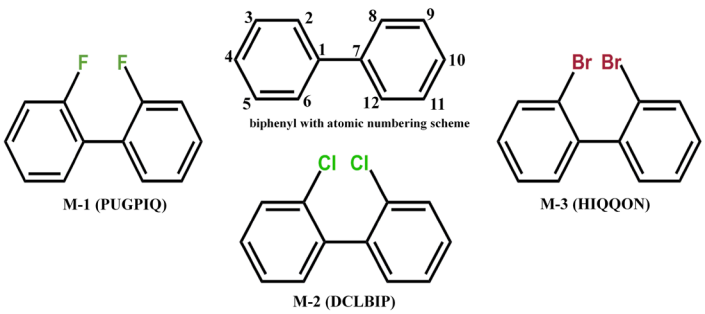

Figure 1: Chemical structure of PUGPIQ (M-1), DCLBIP (M-2) and HIQQON (M-3) with atomic numbering scheme.

Computational details

Quantum chemical calculation

Density functional theory using Gaussian 09 [14] has been used to optimize the ground state molecular geometry of each biphenyl structure in the gas phase by using DFT with the Becke's three-parameter functional that was hybridized with the Lee-Yang-Parr correlation functional (B3LYP) and 6-311 + G (d,p) basis set [15-17]. The optimized structures have been compared with the corresponding X-ray structures, and the quantum chemical calculations and the molecular docking analysis have been performed using the available computational protocols/tools.

Hirshfeld surface analysis

Hirshfeld surface (HS), shape index, curvedness surfaces and the corresponding 2D analysis fingerprints have been carried out using Crystal Explorer 21.5 [18]. The HS is a unique method for visualizing the intermolecular interactions and crystal packing in the crystal [19]. The mapping of Hirshfeld surface over d_{norm} shows a red, blue and white color scheme. The red (d_{norm} is negative) and blue (d_{norm} is positive) colored regions on the surface correspond to contacts that are shorter and longer than van der Waals radii, respectively; the white regions correspond to the contacts that are equal to the van der Waals radii or d_{norm} = 0 [20]. The curvedness map, a function of the root mean square (r.m.s) curvature of the surface, has been drawn and analyzed. The energy framework calculations were performed using molecular wave function at B3LYP/6-11 G(d,p) for a cluster of molecules present within the radius of 3.8 Å. The scale factors used for B3LYP/6-11 G(d,p) energy model is k_{ele} = 1.057, k_{dis} = 0.871, k_{pol} = 0.740 and k_{rep} = 0.618 [21]. Energy frameworks were generated for E_{ele} (red), E_{dis} (green) and E_{tot} (blue) cylinders; the width of each cylinder represents the relative strength of intermolecular packing in different directions [22].

Molecular docking studies

Molecular docking is an important drug design technique to understand the binding pattern of small molecules toward the target protein. The molecular docking binding affinity score for each molecule with Cytochrome-P450-14alpha-sterol demethylase was computed with the help of AutoDock Vina software [23], a suite of automated docking tools (ADT). The target enzyme Cytochrome-P450-14alpha-sterol demethylase PDB file was taken from the protein data bank [24]. The coordinates of grid center for M-1 & M-2 were fixed for docking at X= -17.285814, Y= -7.287279 and Z= 63.722279 (the radius of the grid sphere is 30), whereas the grid centre for M-3 at X= -20.251, Y= -15.279 and Z= -55.222, the radius of the grid sphere being 35. With help of the Discover Studio Visualizer software, the best binding affinity at the active site was visualized for complete ligand-protein interactions [25].

Results and Discussion

Molecular geometry (DFT and X-ray data)

The optimized parameters for the X-ray structures corroborate well with each other within the limits of experimental errors. The optimized structure is shown in Figure 2 and the corresponding data are presented in Table 1. The observable deviation in the bond lengths and bond angles indicate a good correlation between theoretical and experimental values. An overlay of the X-ray and the DFT structure for each molecule is shown in Figure 3. The X-ray and optimized structural data reveal a significant deviation in the position of few ring carbon atoms of M-2 and M-3, including the chlorine atom in M-2. The torsion around the abridging bond C1-C7 in case of all the three di-ortho-substituted-halogenated biphenyls (M-1 = 58.4º, M-2 = 69.2º, M-3 = 84.8º) is different from the reported value of 45º in the gas phase [26]. The dihedral angle between the two phenyl rings for all the three structures (M-1 = 60º, M-2 = 74º, M-3 = 75º) is different when compared with some other similar biphenyls [27-30]. There exist few weak intermolecular interactions C-H-F &C-H-C (M-1), C-H-Cl (M-2) and C-H-Br (M-3), respectively.

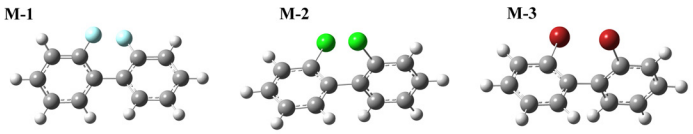

Figure 2: DFT Optimized structures (M-1 to M-3).

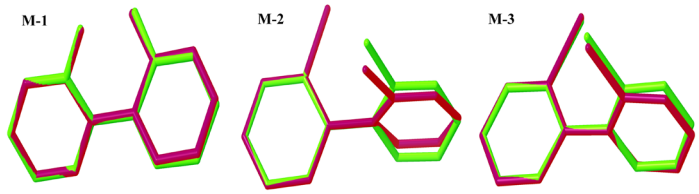

Figure 3: Overlay of X-ray and DFT structure (M-1 to M-3).

Frontier molecular orbital analysis

The frontier molecular orbital energy gap as calculated by BL3YP/6-311 + G(d,p) in case of all the three structures is 5.52 eV, 5.90 eV and 5.80 eV, respectively (Figure 4). The small value of orbital energy gap is indicative of better chemical reactivity and molecular softness while a large value represents low chemical reactivity and high molecular hardness [31,32]. The typically important global reactivity parameters [33] such as chemical hardness (η), chemical softness (σ), electronegativity (χ), electronic chemical potential (μ), global electrophilicity index (ω) and their corresponding values are presented in Table 2. Since the electrophilicity index has been suggested as a possible biological

Table 1: Comparison of experimental and theoretical bond length (Å) and bond angles (º) using DFT method with 6-311 + G(d,p) basis set.

Bondlength (Å)	M-1 (PUGPIQ)		M-2(DCLBIQ)		M-3(HIQQON)	
	XRD	DFT	XRD	DFT	XRD	DFT
C1-C2	1.389	1.389	1.391	1.400	1.388	1.399
C2-C3	1.385	1.385	1.376	1.392	1.369	1.393
C3-C4	1.384	1.384	1.386	1.391	1.378	1.391
C4-C5	1.386	1.386	1.371	1.392	1.373	1.393
C5-C6	1.398	1.399	1.374	1.391	1.365	1.390
C6-C1	1.398	1.398	1.390	1.400	1.402	1.401
C1-C7	1.485	1.485	1.489	1.492	1.499	1.493
C7-C8	1.389	1.389	1.391	1.400	1.379	1.399
C8-C9	1.385	1.385	1.376	1.392	1.371	1.393
C9-C10	1.384	1.384	1.386	1.391	1.383	1.391
C10-C11	1.386	1.386	1.371	1.392	1.376	1.393
C11-C12	1.398	1.398	1.374	1.391	1.371	1.390
C12-C7	1.398	1.398	1.390	1.400	1.382	1.401
Bond Angles (º)						
C1-C2-C3	123.25	122.97	122.37	121.66	122.32	121.66
C2-C3-C4	118.37	118.93	119.27	119.56	119.35	119.56
C3-C4-C5	120.51	119.93	120.00	119.99	119.94	119.99
C4-C5-C6	120.01	119.91	119.60	119.71	120.44	119.77
C5-C6-C1	120.70	121.48	122.57	121.44	121.20	121.47
C6-C1-C2	117.16	116.77	116.17	117.58	116.72	117.54
C2-C1-C7	121.36	122.23	123.03	122.64	122.63	123.02
C6-C1-C7	121.48	120.98	120.75	119.76	120.65	119.41
C1-C7-C8	121.05	122.23	123.03	122.64	122.81	123.02
C1-C7-C12	120.86	120.98	123.03	119.76	119.60	119.41
C7-C8-C9	123.25	122.97	122.37	121.66	122.81	121.66
C8-C9-C10	118.37	118.93	119.27	119.56	118.35	119.56
C9-C10-C11	120.51	119.93	120.00	119.99	120.01	119.99
C10-C11-C12	120.01	119.91	119.60	119.71	120.45	119.77
C11-C12-C7	120.70	121.48	122.57	121.44	120.79	121.47
C12-C7-C8	117.16	116.77	116.17	117.58	117.57	117.54

Table 2: Calculated energy gap and global reactivity descriptors.

Parameters (in eV)	M-1	M-2	M-3
HOMO energy: E_H	-6.78	-6.94	-6.88
LUMO energy: E_L	-1.26	-1.04	-1.08
Energy gap, $\Delta E = \|E_H - E_L\|$	5.52	5.90	5.8
Ionisation potential, $I = - E_H$	6.78	6.94	6.88
Electron affinity, $A = - E_L$	1.26	1.04	1.08
Chemical Hardness, $\eta = \Delta E/2$	2.76	2.95	2.9
Chemical Potential, $\mu = -\chi$	-4.02	-3.99	-3.98
Electronegativity, $\chi = (I + A)/2$	4.02	3.99	3.98
Chemical Softness, $\sigma = 1/2\eta$ $(eV)^{-1}$	0.18	0.17	0.17
Global Electrophilicity, $\omega = \mu^2/2\eta$	2.93	2.70	2.74

descriptor in the development of QSAR [34], the values given in Table 2 may be assumed from this perspective.

Mulliken population analysis

The Mulliken population analysis is a model used for predicting the individual atomic charges and it is highly basis set dependent and unpredictable with small fluctuations in partial charges [35]. The charge on each atom in each structure has been calculated using the B3LYP method with 6-311 + G(d,p) level basic set (Figure 5). All the carbon atoms show a negative charge, except for the atoms C1, C7 (for M-2 and M-3) and C1, C3, C7, C9 for M-1. However, the charge on the hydrogen atoms remains positive. The chlorine atoms show the positive charge, while bromine and fluorine indicate a negative charge.

Molecular electrostatic potential

MEP is the potential that a unit positive charge would experience at any point surrounding the molecule due to the electron density distribution. The MEP analysis performed at the B3LYP/6-311 + G(d, p) level is considered to be predictive of chemical reactivity due to the reason that the regions of negative potential are anticipated to be the sites of protonation and nucleophilic attack, while the regions of positive potential may indicate the location of electrophilic sites [31]. The MEP maps are shown in Figure 6.

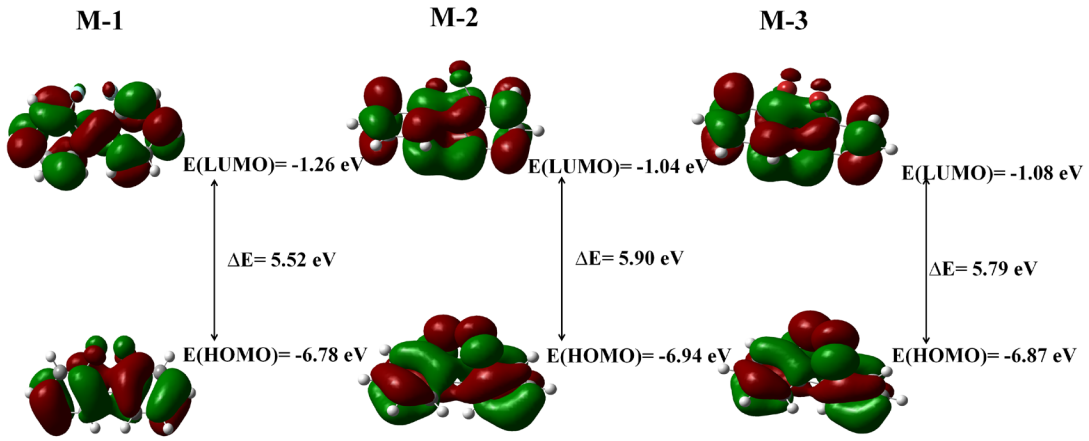

Figure 4: HOMO LUMO energy level and energy gap of M-1to M-3.

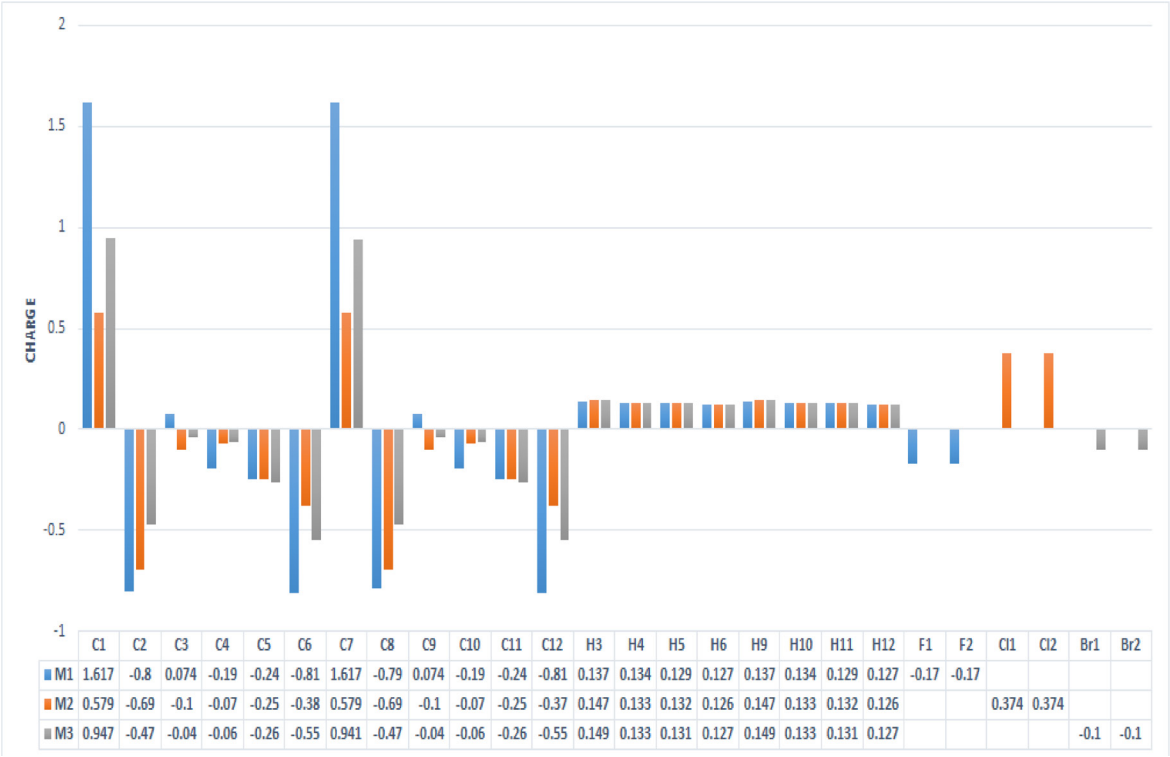

	C1	C2	C3	C4	C5	C6	C7	C8	C9	C10	C11	C12	H3	H4	H5	H6	H9	H10	H11	H12	F1	F2	Cl1	Cl2	Br1	Br2
M1	1.617	-0.8	0.074	-0.19	-0.24	-0.81	1.617	-0.79	0.074	-0.19	-0.24	-0.81	0.137	0.134	0.129	0.127	0.137	0.134	0.129	0.127	-0.17	-0.17				
M2	0.579	-0.69	-0.1	-0.07	-0.25	-0.38	0.579	-0.69	-0.1	-0.07	-0.25	-0.37	0.147	0.133	0.132	0.126	0.147	0.133	0.132	0.126			0.374	0.374		
M3	0.947	-0.47	-0.04	-0.06	-0.26	-0.55	0.941	-0.47	-0.04	-0.06	-0.26	-0.55	0.149	0.133	0.131	0.127	0.149	0.133	0.131	0.127					-0.1	-0.1

Figure 5: Comparison of Mulliken charge analysis of M-1, M-2 and M-3.

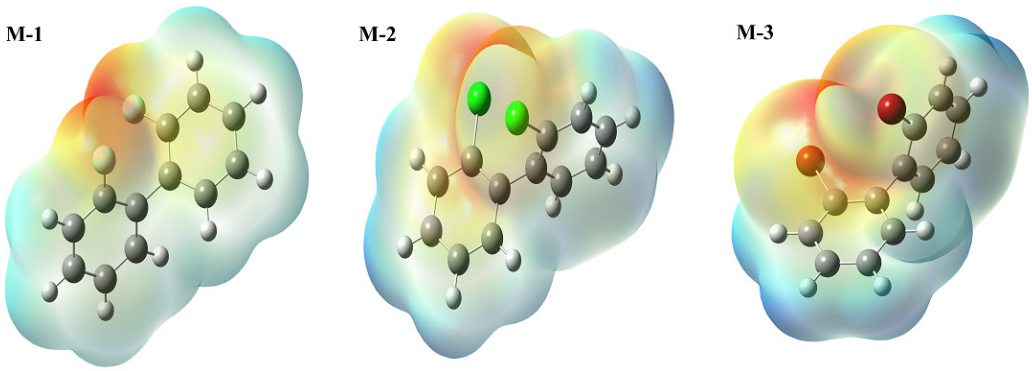

Figure 6: Molecular electrostatic potential of M-1, M-2 and M-3.

The bright red regions are electron-rich and related to electrophilic reactivity while the blue regions are electron-poor regions related to nucleophilic reactivity. In all three cases, the red region over the halogen atoms makes these sites as electron-rich, having an affinity towards the electrophiles. The blue regions over hydrogen atoms of all the benzene rings make these sites electron-poor; thus, having an affinity towards the nucleophiles.

Hirshfeld surface analysis

Figure 7a shows the Hirshfeld surface of M-1, M-2 and M-3 contour over d_{norm}. Three bright and light red spots indicate the existence of C3-H1…F1 and C3-H1…C2 weak interactions in the case of M-1 while the weak interactions (C2-H3…Cl1, C5-H5…Br2) in case of the other two structures are also represented by the usual colour scheme. The topography of the shape-index and curvedness plot for all the three structures indicates the presence of insignificant π-π interaction. (Figure 7 b,c).

The two-dimensional fingerprint plots (Figure 8) indicate the percentage contribution of intermolecular interactions and to the total Hirshfeld surface area [36]. The interaction contribution due to H...Cl (38.8%) and H...Br (37.5%) contacts is almost identical when compared with that of H...F (30.8%) contacts. The strong intermolecular interactions appear as distinct spikes in the fingerprint plots. The hydrogen-halogen interaction appears as two characteristic wings having a significant contribution to the crystal packing in each structure.

Energy framework analysis

The topology of pair-wise intermolecular interaction energies in each structure enables the construction of energy frameworks, viz. Electrostatic (E_{ele}), Dispersion (E_{dis}), Repulsion (E_{rep}), Polarization (E_{pol}) and Total (E_{tot})energy (Table 3) [37]. The purple-colored molecule in M-1 (with symmetry operation: x, y, z and located at a distance of 5.79 Å from the centroid) indicates the maximum total interaction energy (−19.4 kJ/mol), while the turquoise-colored molecule (with symmetry operation: -*x* + 3/4, y+ 3/2, z + ¼ and located at a distance of 7.79 Å) gives the lowest total interaction energy (−4.8 kJ/mol). Similarly, in case of M-2 and M-3, the maximum and minimum total energies are −14 kJ/mol, −4.4 kJ/mol and −23.6 kJ/mol, −5.3 kJ/mol, respectively. The dispersion energy (E_{dis}) rule over the electrostatic energy (E_{ele}) in case of all three molecules and its graphical visualization is depicted in Figure 9 (along z-axis).

Molecular docking analysis

Hydrogen bonding plays a significant role in the structural and biological function of the drug molecules, and hence the ligand-receptor interactions were examined on the basis of hydrogen bonding [38]. Table 4 contains the binding energy, its type and other details for each structure with Cytochrome P450 14alpha-sterol demethylases (CYP51). The M-1:1EA1 complex is stabilized by one hydrogen and halogen bond and four hydrophobic bonds. The fluorine atom of M-1 is bonded to the hydrogen atom of active amino acid ARG96 (distance = 2.7469 Å) and the molecular

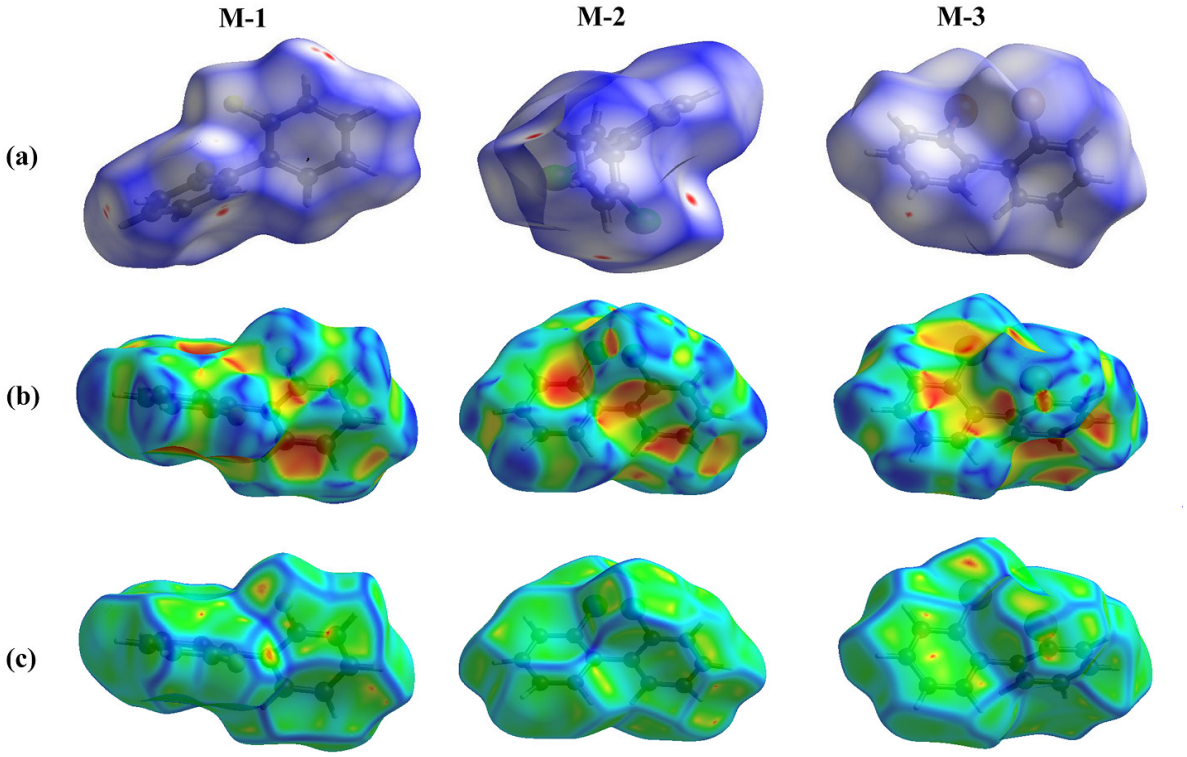

Figure 7: Hirshfeld surface images of (a) d_{norm}, (b) Shape-index (c) Curvedness for M-1, M-2, M-3.

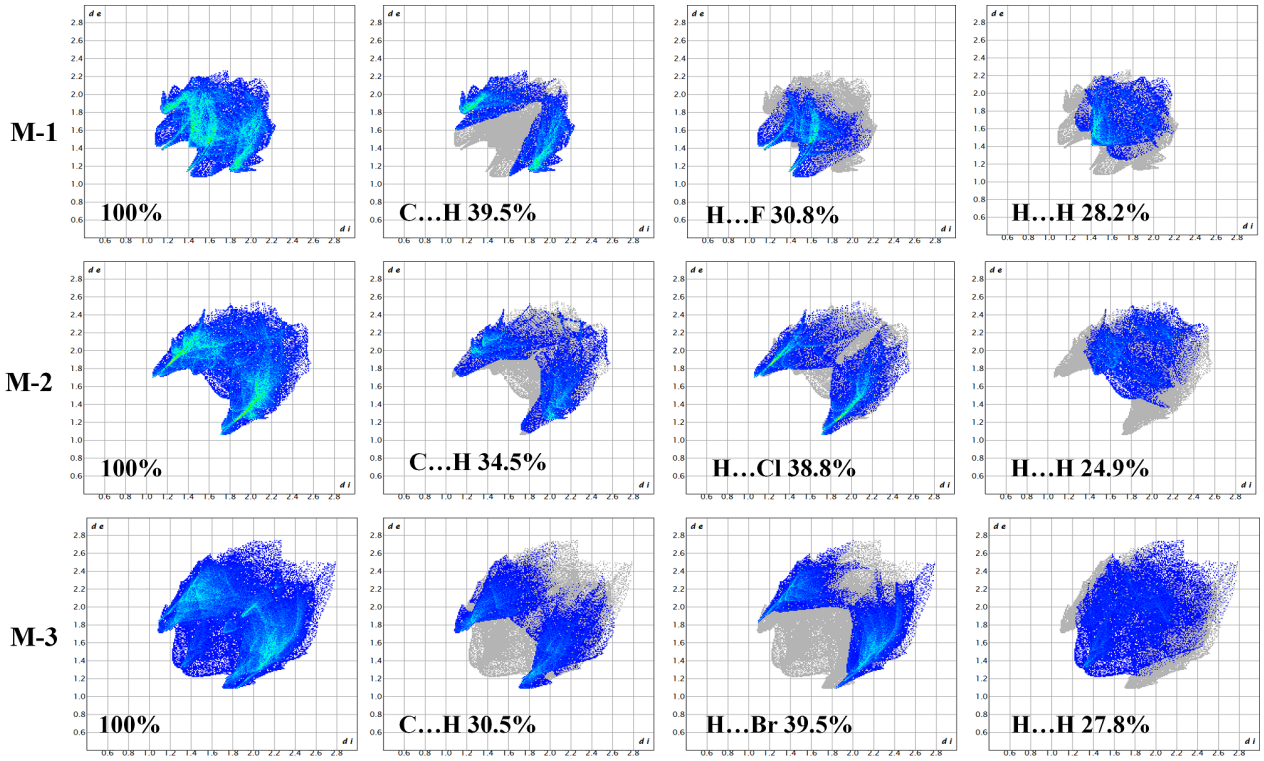

Figure 8: 2D Fingerprint plot with d_{norm} view showing close contacts of M-1, M-2 and M-3.

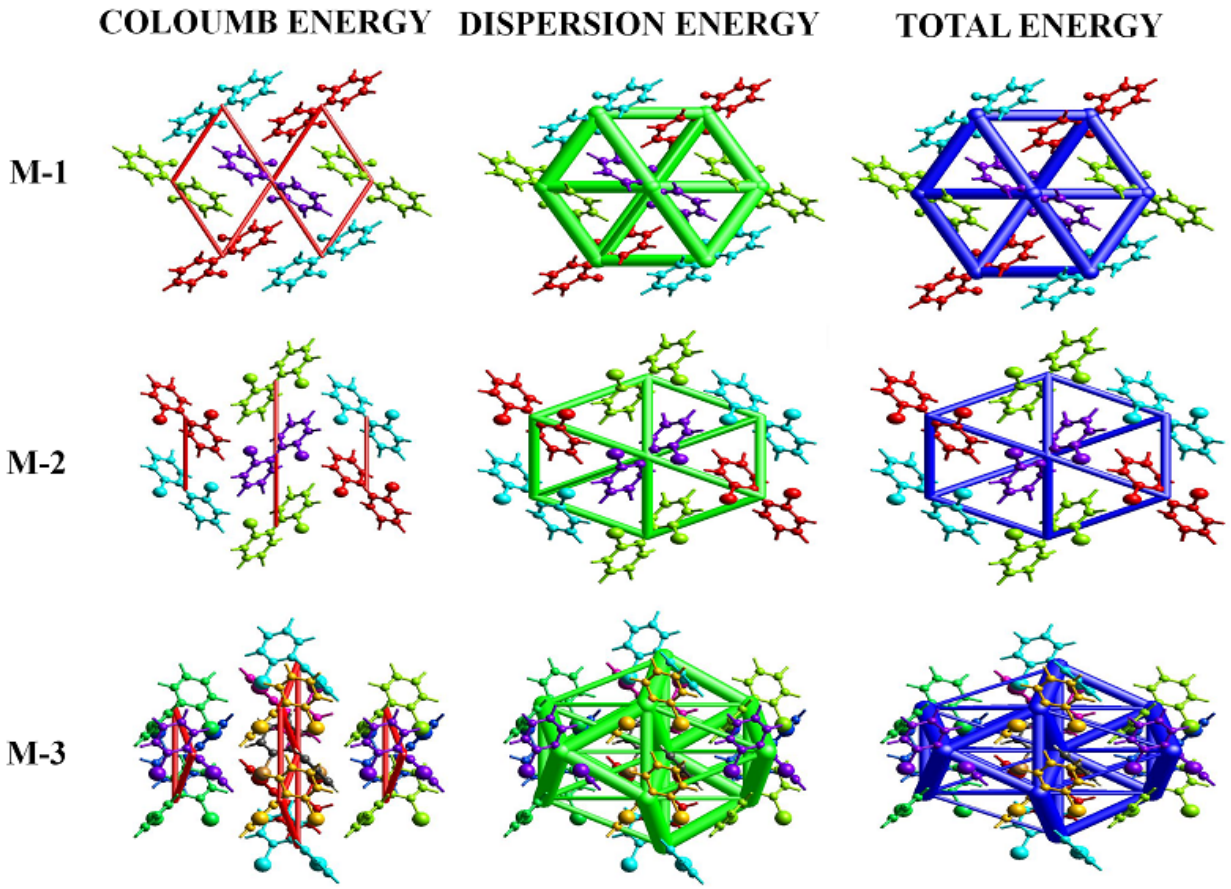

Figure 9: Graphical representation of electrostatic interactions: coulomb interaction energy (red), dispersion energy (green), and total interaction energy (blue) for each structure along the z- axis.

Table 3: Interaction energies in kJ/mol using B3LYP/6-31 G(d,p) method.

M1									
	N	Symmetry operation	R	Electron Density	Eele	Epol	Edis	Erep	Etot
	4	-x+3/4,y+3/4,z+1/4	6.83	B3LYP/6-31G(d,p)	-5.2	-0.7	-21.4	14.2	-15.8
	4	x+1/2,y,z+1/4	7.07	B3LYP/6-31G(d,p)	3.4	-0.8	-18.6	9.9	-14.2
	4	-x+3/4,y+3/4,z+1/4	7.97	B3LYP/6-31G(d,p)	0.6	-0.4	-7.7	2.5	-4.8
	2	x,y,z	5.79	B3LYP/6-31G(d,p)	-5.6	-1.3	-24.0	13.4	-19.4
Total					-13.6	-3.2	-71.7	40	-54.2
M2									
	N	Symmetry operation	R	Electron Density	Eele	Epol	Edis	Erep	Etot
	4	-x+3/4, y+3/4, z+1/4	8.48	B3LYP/6-31G(d,p)	-1.4	-0.4	-7.7	6.5	-4.4
	4	x+1/2, y, z+1/4	7.51	B3LYP/6-31G(d,p)	-4.5	-0.8	-17.5	10.7	-14.0
	4	-x+3/4, y+3/4, z+1/4	7.06	B3LYP/6-31G(d,p)	-3.3	-0.7	-18.0	10.7	-13.1
	2	x, y, z	6.64	B3LYP/6-31G(d,p)	-2.8	-0.8	-13.7	6.2	-11.7
Total					-12	-2.7	-56.9	34.1	-43.2
M3									
	N	Symmetry operation	R	Electron Density	Eele	Epol	Edis	Erep	Etot
	1	-x, -y, -z	5.40	B3LYP/6-31G(d,p)	-4.4	-1.0	-22.1	18.1	-13.5
	2	-x, y+1/2, -z+1/2	6.89	B3LYP/6-31G(d,p)	-7.5	-1.0	-28.4	16.0	-23.6
	2	-x+1/2, y+1/2, z	7.37	B3LYP/6-31G(d,p)	-2.5	-0.8	-21.6	11.2	-15.2
	2	-x+1/2, y+1/2, z	8.57	B3LYP/6-31G(d,p)	-0.9	-0.4	-9.3	6.6	-5.3
	2	x, y, z	7.46	B3LYP/6-31G(d,p)	-6.3	-0.9	-16.9	14.3	-13.2
	2	x+1/2, -y+1/2, -z	8.81	B3LYP/6-31G(d,p)	-1.8	-0.2	-5.4	2.2	-5.5
	2	x+1/2, y, -z+1/2	9.09	B3LYP/6-31G(d,p)	-1.2	-0.3	-6.4	2.8	-5.3
	1	-x, -y, -z	7.48	B3LYP/6-31G(d,p	-8.7	-1.4	-27.6	21.5	-20.9
Total					-33.3	-60	-137.7	-92.7	-65.4

Table 4: Binding energy, Hydrogen bond, Electrostatic & Hydrophobic contacts of PUGPIQ, DCLBIP and HIQQON with Cytochrome P450 14alpha-sterol demethylases.

Inhibtor	B.E (Kcalmol^{-1})	Interactions	Distance (Å)	Bonding	Bonding types
PUGPIQ	-7.2	ARG96 [HH21…F]	2.7469	Hydrogen	Conventional hydrogen bond
		ARG96 [CZ...F]	3.6726	Halogen	Halogen acceptor
		PHE83 [π...π]	5.3783	Hydrophobic	π-π T-shaped
		PHE255 [π...π]	5.0189	Hydrophobic	π-π T-shaped
		LEU100 [CB... π]	5.0507	Hydrophobic	π-Alkyl
		ALA256 [CB… π]	4.1314	Hydrophobic	π -Alkyl
DCLBIP	-7.6	LEU321 [CD1… π]	3.95856	Hydrophobic	π -Sigma
		TYR76 [π …Cl2]	3.84652	Hydrophobic	π -Sigma
		TYR76 [π … π]	5.1247	Hydrophobic	π-π T-shaped
		HIS259 [π …Cl1]	4.69456	Hydrophobic	π -Alkyl
HIQQON	-7.5	ARG96 [NH2...BR]	3.34	Hydrogen	Conventional hydrogen bond
		ARG96 [NH2...π]	4.84	Electrostatic	π-Cation
		ALA256 [CB...π]	3.98	Hydrophobic	π- Sigma
		PHE255 [π...π]	5.21	Hydrophobic	π-π T shaped
		MET79 [BR...CB]	3.64	Hydrophobic	Alkyl
		TYR76 [π...BR]	5.20	Hydrophobic	π-Alkyl
		PHE83 [π...BR]	5.24	Hydrophobic	π-Alkyl
		MET79 [BR....π]	5.11	Hydrophobic	π-Alkyl
		LEU321 [CB...π]	5.33	Hydrophobic	π-Alkyl
		LEU100 [CB... π]	5.13	Hydrophobic	π-Alkyl

docking score with 1EA1 is -7.2 Kcal/mol. Two hydrophobic bonds have been observed between Cl2, Cl1 and TYR76, HIS259 rings, respectively, in case of M-2. The benzene ring makes a bifurcated hydrophobic bond with TYR76 and LEU321 residue and the molecular docking score with 1EA1 is -7.6 Kcal/mol.

The M-3:1EA1 complex is stabilized by one hydrogen, one electrostatic and eight hydrophobic bonds. The donor hydrogen atom of the residue ARG96 interacts with the halogen atom (bromine) of the ligand at a distance of 3.34 Å. The electrostatic interaction (π-cation) is exhibited by the six-membered ring of M-3 bonded with the hydrogen atom of active amino acid ARG96 (distance = 4.84 Å). The hydrophobic interactions (π-Sigma) and (π -π T-shaped) are bonded by the six-membered ring with a carbon atom and benzene rings of active amino acids ALA256 and PHE255 (distance = 3.98 Å and 5.21 Å, respectively). The alkyl

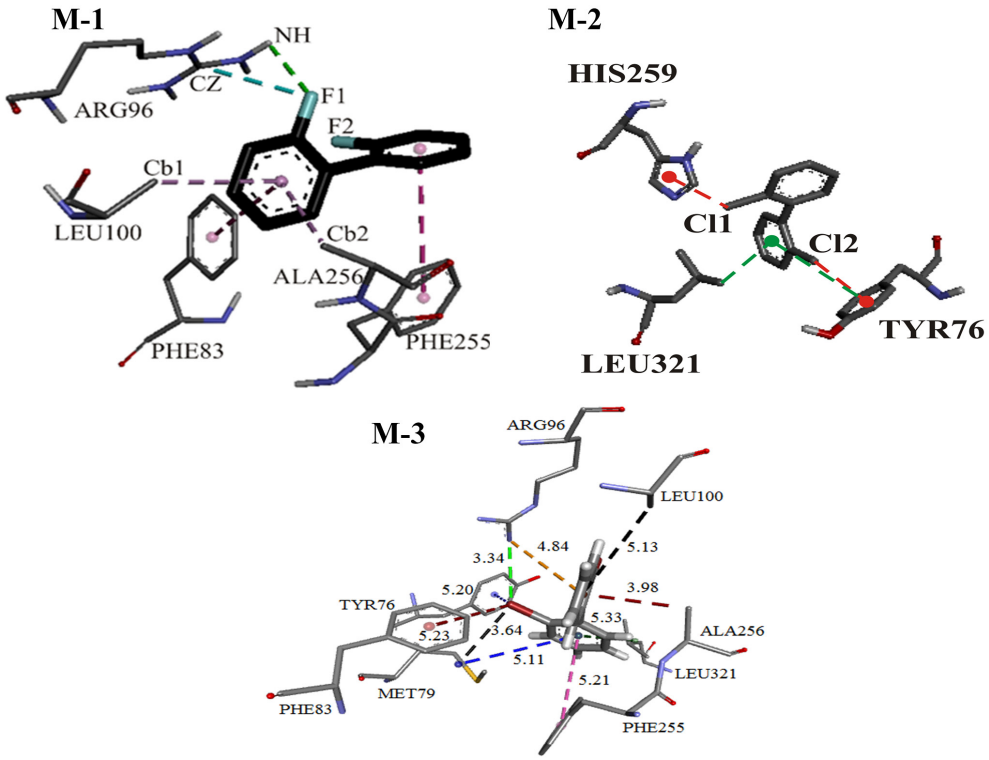

Figure 10: Molecular interaction of each structure with 1EA1 binding site.

hydrophobic interaction leads to the formation of bond between the bromine and carbon atoms of the active enzyme MET79 (distance = 3.64 Å). The π-alkyl of the hydrophobic interactions are bonded between the benzene ring of the active enzymes TYR76 and PHE83 with the bromine atom of the ligand (distance = 5.20 Å and 5.24 Å, respectively). Similarly, the other three hydrophobic (π-Alkyl) interactions as exhibited by the benzene ring are shown bonded with the carbon atom of the corresponding active protein sites MET79, LEU321 and LEU100 at a bonding distance of 5.11Å, 5.33 Å and 5.13 Å, respectively. The molecular docking score of M-3 with 1EA1is -7.5 Kcal/mol. The molecular binding interactions in case of each complex are shown in Figure 10.

Conclusions

The theoretical investigations on the crystal structures of di-ortho-substituted halogenated biphenyls, their Hirshfeld surface, and molecular docking analysis embodies the work reported here. The DFT geometry of each structure, by and large, is in sync with the X-ray data. The DFT investigations provide some useful insights about the molecular structure, atomic Mulliken charges, molecular electrostatic potential and HOMO-LUMO energy gaps in case of each biphenyl. The frontier molecular orbital investigations indicate that M-1 is more favourable for charge transfer as compared to M-2 and M-3. The HS analysis reveals the existence of weak C-H-F, C-H-C (M-1) and C-H-Cl and C-H-Br interactions in M-2 and M-3. Representing a significant contribution of dispersion component in each molecule, the 3D energy frameworks analysis indicates the dominance of dispersion energy over the electrostatic component. *In-silico* molecular docking results against Cytochrome P450 14alpha-sterol demethylases with significant binding score show the inhibitory activity of each molecule against the fungal growth. Hence, the three di-ortho-substituted halogenated biphenyls could be used in antifungal drug design.

Acknowledgement

Rajni Kant acknowledges the Research Grants as sanctioned under the RUSA 2.0 Project (Ref.No: RUSA/JU/2/2019-20/111/3588-3636). Neha Kumari acknowledges the UGC for a Fellowship as sanctioned under the NFSC scheme (Ref No.F.82-1/2018 (SA-III)) by the Government of India.

References

1. Sharma N, Prashanth T, Lakshmi Ranganatha V, et al. Crystal structure of 2, 4, 6-triisopropyl-2', 5'-dimethoxybiphenyl. Crystallogr Rep. 2015; 60: 1116-1120.
2. Jain ZJ, Gide PS, Kankate RS. Biphenyls and their derivatives as synthetically and pharmacologically important aromatic structural moieties. Arab J Chem. 2017; 10: S2051-S2066.
3. Rikhi M, Hoda S, Nagpal S, et al. Antifungal activity of biphenyl-2,6-diethanone derivatives. Int J Pharm Pharm Sci. 2016; 8: 378-380.
4. Kant R, Gupta VK, Kumar A, et al. Crystallography of 4, 4 - Bis-(nPropylamino) - Biphenyl [C18N2H24]. Mol Cryst Liq Cryst. 2006; 233: 237-242.
5. Zhang SJ, Xiang H, Rao GW, et al. Crystal structures of two 4-phenylbenzophenones. J Struct Chem. 2013; 54: 779-786.
6. Gobbi S, Cavalli A, Negri M, et al. Imidazolylmethyl-benzophenones as highly potent aromatase inhibitors. J Med Chem. 2007; 50: 3420-3422.

7. Ribeiro PR, Ferraz CG, Guedes ML, et al. A new biphenyl and antimicrobial activity of extracts and compounds from Clusia burlemarxii. Fitoterapia. 2011; 82: 1237-40.
8. Ding Y, Mao L, Xu D, et al. C-Aryl glucoside SGLT2 inhibitors containing a biphenyl motif as potential anti-diabetic agents. Bioorganic & Medicinal Chemistry Letters. 2015; 25: 2744-2748.
9. Rathi BS, Wagh NK, Bodhankar SL, et al. Evaluation of anti-inflammatory and analgesic activity of a new class of biphenyl analogs in animal models of inflammation. Arzneimittelforschung. 2006; 56: 640-646.
10. Lee YJ, Yang JH. Chlorination of ortho-position on polychlorinated biphenyls increases protein kinase C activity in neuronal cells. Toxicological research. 2012; 28: 107-112.
11. Aldridge B, De Luca G, Edgar M, et al. The structure of 2, 2'-difluorobiphenyl in solid crystalline and liquid crystalline phases. Liquid crystals. 1998; 24: 569-581.
12. Romming C, Seip HM, Oymo I. Structure of gaseous and crystalline 2, 2'–Dichlorobiphenyl. Acta Chem. Scand. 28a 1974; 28: 507-514.
13. MacNeil DD, Decken AN. 2, 2'-Dibromobiphenyl. Acta Crystallographica 1999; C55: 628-630.
14. Frisch MJ, Trucks GW, Schlegel HB, et al. Gaussian 09; Gaussian, Inc. Wallingford, CT, 2009; 32: 5648-5652.
15. Becke AD. A half-half theory of density functionals. J. Chem. Phys. 1993; 98:1372.
16. Lee BS. Causal relations among stock returns, interest rates, real activity, and inflation. J Finance. 1992; 47: 1591-1603.
17. Choi CH, Kertesz M. Conformational information from vibrational spectra of styrene, trans-stilbene, and cis-stilbene. Journal Phys Chem. A. 1997; 101: 3823-3831.
18. Spackman PR, Turner MJ, McKinnon JJ, et al. CrystalExplorer: a program for Hirshfeld surface analysis, visualization and qu¬antitative analysis of molecular crystals. J Appl Cryst. 2021; 54: 1006-1011.
19. Maity T, Mandal H, Bauzá A, et al. Quantifying conventional C–H··· π (aryl) and unconventional C–H··· π (chelate) interactions in dinuclear Cu (II) complexes: experimental observations, Hirshfeld surface and theoretical DFT study. New J Chem. 2018; 42: 10202-10213.
20. McKinnon JJ, Jayatilaka D, Spackman MA. Towards quantitative analysis of intermolecular interactions with Hirshfeld surfaces. Cryst Engg Comm. 2007; 37: 3814-3816.
21. Mackenzie CF, Spackman PR, Jayatilaka D, et al. Crystal Explorer model energies and energy frameworks: extension to metal coordination compounds, organic salts, solvates and open-shell systems. IUCrJ. 2017; 4: 575-587.
22. Hema MK, Renganathan RA, Swamy SN, et al. 4, 4, 4-Trifluoro-1-(thiophen-2-yl) butane-1, 3-dione nickel (II) complex: Synthesis, structure, quantum chemical and DNA binding studies. J Mol Struct. 2020; 1202: 127277.
23. Morris GM, Huey R, Lindstrom W, et al. J Compt Chem. 2009; 30: 2785-2791.
24. Rcsb Pdb-1EA1: Cytochrome P450 14 alpha-sterol demethylase (CYP51) from Mycobacterium tuberculosis in complex with fluconazole.
25. BIOVIA discovery studio visualizer. Software version. 2016. 20, 779.
26. Popelier PL, Maxwell PI, Thacker JC, et al. A relative energy gradient (REG) study of the planar and perpendicular torsional energy barriers in biphenyl. Theor Chem Acc. 2019; 138: 1-6.
27. Rajnikant, Watkin DJ, Tranter G. 4-Benzylbiphenyl. Acta Crystallographica 1995; C51: 2388-2390.
28. Rajnikant, Watkin DJ, Tranter G. Disordered Fluorine in 2-Fluorobiphenyl. Acta Crystallographica 1995; C51: 1452-1454.
29. Rajnikant, Watkin DJ, Tranter G. 3-Nitrobiphenyl. Acta Crystallographica 1995; C51: 2071-2073.
30. Rajnikant, Watkin DJ, Tranter G. Biphenyl-2-methanol. Acta Crystallographica 1995; C51: 2161-2163.
31. Drissi M, Benhalima N, Megrouss Y, et al. Theoretical and experimental electrostatic potential around the m-nitrophenol molecule. Molecules. 2015; 20: 4042-4054.
32. Pearson RG. Chemical hardness and density functional theory. J Chem Sci. 2005; 117: 369-377.
33. Bayannavar PK, Sannaikar MS, Kumar SM, et al. Synthesis, X-ray characterization, DFT studies and Hirshfeld surface analysis of new organic single crystal: 2-(4-Methoxyphenyl)-4-{[2'-(1H-tetrazol-5-yl) biphenyl-4-yl] methyl}-2, 4-dihydro-3H-1, 2, 4-triazol-3-one (MTBT). J Mol Struct. 2019; 1179: 809-819.
34. Parthasarthi R, Subramanian V, Roy DR, et al. Electrophilicity indexes as possible descriptors of biological activity. Bioorg. Med. Chem. 2004; 12: 5533-5543.
35. Rigby J, Izgorodina EI. Assessment of atomic partial charge schemes for polarisation and charge transfer effects in ionic liquids. Phys Chemi Chem Phys. 2013; 15: 1632-1646.
36. Seth SK. Structural characterization and Hirshfeld surface analysis of a CoII complex with imidazo [1, 2-a] pyridine. Acta Crystallographica. 2018; E74: 600-606.
37. Kumar SM. 3D energy frameworks of dimethylbenzophenone tetramorphs. Heliyon. 2019; 5: e01209.
38. Saminathan M, Jayakumar MR, Chandrasekaran R, et al. Synthesis, spectral, crystal structure, drug-likeness, in silico, and in vitro biological screening of halogen [Cl, Br] substituted N-phenylbenzo [g] indazole derivatives as antimicrobial agents. J Heterocycl Chem. 2021; 58: 841-863.